Directional Local Density of States of Classical and Quantum Propagating Surface Plasmons

Martin Berthel, Quanbo Jiang, Aline Pham, Joël Bellessa, Cyriaque Genet, Serge Huant, Aurelien Drezet

Local Density of States of Classical and Quantum Propagating Surface Plasmons

Martin Berthel,[1] Quanbo Jiang,[1] Aline Pham,[1] Joel Bellessa,[2] Cyriaque Genet,[3] Serge Huant,[1] and Aurélien Drezet[1,*]

[1]*Institut Néel, CNRS and Université Joseph Fourier, B.P. 166, 38042 Grenoble Cedex, France*

[2]*Institut Lumière Matière, UMR5306 Université Lyon 1-CNRS, Université de Lyon, 69622 Villeurbanne cedex, France*

[3]*ISIS, UMR 7006, CNRS-Université de Strasbourg, 8 allée Monge, 67000 Strasbourg, France*

(Received 25 May 2016; revised manuscript received 10 October 2016)

We theoretically and experimentally introduce the concept of the local density of states (LDOS) associated with propagative surface plasmons (PSPs) launched along a structured thin gold film (a concept we call PSP LDOS). The alternative method couples a near-field optical microscope, in either the classical or the quantum regime of excitation, to a far-field leakage-radiation microscope. This method allows for selecting and collecting a very narrow portion of the directional SP wave vectors, thereby offering sufficient resolution to probe the collimation efficiency of a SP beam for a source near the focal point of a Bragg parabolic reflector. We are able to build and image the PSP LDOS in a fully integrated quantum SP launcher by depositing a diamond nanocrystal hosting nitrogen-vacancy centers at the focal point of the mirror. Our demonstration of the PSP LDOS with quantized SPs offers alternative prospects in the field of quantum plasmonics.

DOI:

I. INTRODUCTION

Controlling the emission of a pointlike dipole in a complex environment is a central issue for nanophotonics and nanoplasmonics [1–6]. In this context, the key quantity to be measured is the local density of states (LDOS), which generalizes the concept of the Purcell factor [7]. The LDOS defines the ability of a dipole to populate the various optical modes available in a given environment [8,9]. Since the environment is complex in nanophotonics, both in composition and geometry, the LDOS strongly depends on the dipole location and orientation. This dependence entails the peculiar role played by evanescent waves dressing the objects. In recent years, the photonic LDOS was explored in nanostructures supporting resonant or localized surface plasmon (LSP) modes by means of near-field optical microscopes (NSOMs) [10,11] that allow for an acute position control of a dipolar pointlike tip in the optical near field [12–14]. Alternative powerful methods have been developed to record these LSP-LDOS near-metal nanoparticles [15–18], colloidal-particle networks [19], or single nanoholes [20]. However, to date, no method has been proposed to operate precise studies of propagative SP (PSP) LDOS on extended and nanostructured metal-dielectric planar systems, where propagating SPs are natural information vehicles for photons along micrometers. Since propagative SPs offer a range of technological applications for two-dimensional information transfer, it becomes crucial to define a protocol for recording PSP LDOS. This issue is the first to be considered in this article. Moreover, in the context of quantum-information processing, one would ultimately like to control and map these PSP LDOS using a quantum fluorescent emitter scanning over the plasmonic system [21]. This knowledge is indeed particularly relevant since current research focuses on the coupling of quantum emitters to metal nanoantennas [10,14], waveguides [1,22], or structured metal films [23,24], for the ultimate purpose of developing fully integrated and optimized single-SP sources. This issue is the second one that we tackle in this work.

In this article, we introduce a general experimental and theoretical scheme for mapping the PSP LDOS in extended and planar devices using a NSOM coupled to resolved back-focal-plane imaging [see Fig. 1(a)]. We demonstrate that this association provides the high contrast and resolution needed for PSP-LDOS measurements. As a second step, we exploit the PSP-LDOS protocol to implement an optimized SP collimator working in the quantum regime. For the purpose of this work, we consider two types of NSOM probes, made of either a classical 100-nm aperture tip or a quantum nitrogen-vacancy- (NV) based optical tip. The latter [25] provides a way to accurately position a single-photon source in a complex environment, spatially limited by the 80-nm nanodiamond that hosts the NVs. Both sorts of tips are placed in the near field of a gold film to convert the light they emit into propagative SPs. In order to map the SP propagation, we use a leakage-radiation microscope (LRM) that records the coupled light transmitted through the thin metal layer in the glass substrate [24,26–31]. Briefly, an elementary SP characterized by its in-plane wave vector $\mathbf{k}_{SP}$ leaks into the glass [see Fig. 1(a)] and couples to light of in-plane wave vector $\mathbf{k}$, matching the

*aurelien.drezet@neel.cnrs.fr

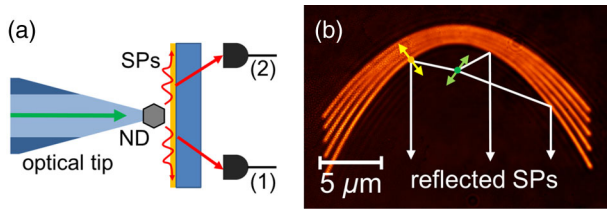

FIG. 1. Principle of the experiment. (a) Either a classical-aperture NSOM tip (not shown here) or an active NV-based NSOM tip excites SPs on a 50-nm-thick gold film evaporated on a glass substrate. Leakage radiation of the emitted SPs in the Fourier plane (1) in a given direction or (2) collected with a high-numerical-aperture (NA) microscope objective. (b) Image of the direct plane of the structured gold film in transmission under global illumination. Five confocal parabolic slits, each of 150 nm width, are milled by a FIB. Most SPs emitted by a dipole located at the focus point (the green double arrow) are reflected in the same direction by the parabolas' induced dipoles (the yellow double arrow), giving a collimated SP beam.

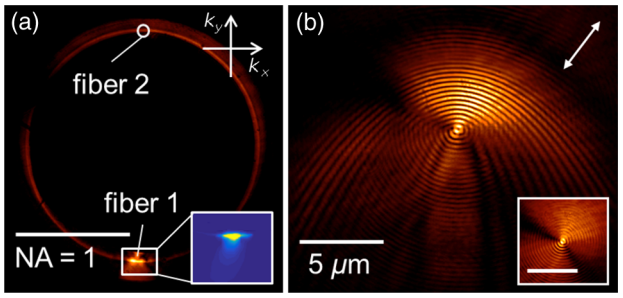

FIG. 2. LRM images [recorded, respectively, in the (a) Fourier and (b) direct planes] with a classical NSOM tip facing the gold film at the focus of the parabolas. The inset in (a) is an enlargement of the simulation for the Fourier-plane zone collected by fiber 1. The inset in (b) is a LRM image obtained with the same NSOM tip along the plain metal film (500 nm is the scale bar for the inset). In (a) NA stands for numerical aperture. In (b), a double white arrow indicates the dipole orientation. The closest parabola to the focus point F is represented by a white dashed curve.

real part of $\mathbf{k}_{\mathrm{SP}}$. Leaky waves are emitted at the fixed angle Θ_{LRM} defined by the condition $\mathrm{Re}[k_{\mathrm{SP}}] = (2\pi/\lambda) n_g \sin(\Theta_{\mathrm{LRM}})$ (where n_g is the glass-substrate optical index and λ the optical wavelength). Being a far-field method, a LRM is powerful in mapping SP propagation over a metal film and has been applied in the context of quantum plasmonics, i.e., for the demonstration of single-SP launching, a wave-particle-duality test, and a measurement of second-order temporal and spatial coherence [23,32]. Furthermore, the LRM also provides a way for determining the plane-wave angular spectrum associated with the intensity distribution $I_{\mathrm{SP}}(\mathbf{k}_{\mathrm{SP}})$ in the Fourier space [24,26,29–31]. This approach defines a methodology for mapping the PSP LDOS in the $\mathbf{k}_{\mathrm{SP}}$ space, as demonstrated below.

II. PROOF OF PRINCIPLE

The plasmonic device we consider is a Bragg parabolic mirror [28] made of five confocal slits (each with a 150 nm width) milled using a *focused ion beam* (FIB) in a 50-nm-thick gold film. The Bragg condition is such that a pointlike source located near the focus excites propagative SPs subsequently reflected along the symmetry axis of the in-plane mirror. An optical image of the structure recorded using a far-field illumination is displayed in Fig. 1(b).

Prior to going to the PSP-LDOS measurements, it is necessary to interpret the LRM images of the parabolic reflector (see also Ref. [32]), first with the classical tip used for excitation ($\lambda_{\mathrm{exc}} = 633$ nm). Typical LRM images recorded by a camera capturing the SP propagation in the Fourier plane of an oil-immersion objective are displayed in Fig. 2(a) and in the direct image plane in Fig. 2(b). The tip is located above the metal film (the tip-surface distance is kept at $h \simeq 20$ nm) near the parabolas' common focus F. The thin ring observed in the Fourier plane is the typical signature of the leaky SPs launched by the NSOM tip [26]. In the direct plane, the 2D profile shows a SP wave generated by an in-plane electric dipole which is also visible in Fig. 2(a) as an anisotropy in the radiation profile. When the tip is positioned at F, the emitted SPs reflected by the Bragg mirror are strongly collimated along a specific $\mathbf{k}$ direction [see Fig. 2(a)]. The same behavior is observed in the direct-plane image as shown in Fig. 2(b), where several fringes are also superposed to the initial SP wave induced by the NSOM tip for SPs launched by the same NSOM tip on a plain gold film [see the inset of Fig. 2(b)].

In order to theoretically describe LRM images, we use a modal expansion into transverse-magnetic (TM) and -electric (TE) waves [24,29]. Considering an oscillating pointlike electric dipole $\boldsymbol{\mu} e^{-i\omega t}$ (with $(\omega/c) = (2\pi/\lambda)$) located at a height h above the air-gold interface, we express the radiated intensity in the Fourier plane as a function of the in-plane wave vector $\mathbf{k}$ of the radiated light. Here, the TM term dominates [24,29] and we have

$$I_{\mathrm{TM}}(\mathbf{k}) \simeq \eta \left| \frac{\boldsymbol{\mu} \cdot \hat{\mathbf{z}}}{\sqrt{\left(\frac{2\pi}{\lambda}\right)^2 - k^2}} - \frac{\boldsymbol{\mu} \cdot \mathbf{k}}{k^2} \right|^2 F_{\mathrm{SP}}(\mathbf{k}), \qquad (1)$$

where $\hat{\mathbf{z}}$ is a unit vector along the z-optical axis, η is an overall detection efficiency taking into account the transmission of the microscope objective, and $F_{\mathrm{SP}}(\mathbf{k})$ is a resonant SP Lorentzian profile [29]. In order to simulate the Fourier-plane image of Fig. 2(a), we coherently add to the field generated by the NSOM tip the contribution due to the Bragg mirror. We describe this additional term as a sum of N elementary electric dipoles $\boldsymbol{\mu}_p$ $(p = 1, 2, \ldots, N)$ obtained by discretizing the parabolic mirrors (the method is explained in Ref. [24]). Each $\boldsymbol{\mu}_p$ is excited by the SP

field $\mathbf{E}_{\mathrm{SP}}(\mathbf{x}_p, \mathbf{x}_0)$ acting at the dipole location $\mathbf{x}_p := [x_p, y_p, z_p = 0]$, while the tip is located at $\mathbf{x}_0 := [x_0, y_0, h]$. We model the coupling between $\boldsymbol{\mu}_p$ and $\mathbf{E}_{\mathrm{SP}}(\mathbf{x}_p, \mathbf{x}_0)$ by a linear relation $\boldsymbol{\mu}_p = \xi[\mathbf{E}_{\mathrm{SP}}(\mathbf{x}_p, \mathbf{x}_0) \cdot \hat{\mathbf{n}}_p]\hat{\mathbf{n}}_p$ where ξ is a constant polarizability and $\hat{\mathbf{n}}_p$ is an in-plane unit vector oriented along the normal to the parabola at $\mathbf{x}_p$.

We present, in the inset of Fig. 2(a), an enlargement of the simulated back-focal-plane image [24,29] obtained with the tip located at the parabola focus. It is in a very good agreement with the experiment.

We now turn on to the PSP-LDOS demonstration. The principle [32] is sketched in Fig. 1(a). The tip brought in the near field of the metallic film shines on SPs, which leak and are recorded in the Fourier plane. Subsequently, after selecting and detecting only light leaking along a specific wave-vector direction, we map the partial PSP LDOS associated with this wave vector by scanning the tip while maintaining the detection direction fixed in the Fourier plane. As shown below, we unambiguously define the partial PSP LDOS with a high $\mathbf{k}$ resolution in the Fourier space.

For this purpose, it is worth remembering that the full LDOS $\rho_{\mathrm{LDOS}}(\omega, \mathbf{x}_0)$ associated with a dipole $\boldsymbol{\mu} e^{-i\omega t}$ is given by [8,12,33]

$$\rho_{\mathrm{LDOS}}(\omega, \mathbf{x}_0) = \frac{3}{\pi\omega^2|\boldsymbol{\mu}|^2} P(\omega, \mathbf{x}_0), \tag{2}$$

where $P(\omega, \mathbf{x}_0)$ is the total energy rate of the oscillating dipole (including radiative and nonradiative exchanges with the environment). For a simple two-level quantum emitter [33], we have $P(\omega, \mathbf{x}_0) = \hbar\omega\Gamma(\omega, \mathbf{x}_0)$, where Γ is the full decay rate including dissipation in the metal. As the LRM only accounts for radiative SP modes, we define the partial PSP LDOS by integrating the radiative power along a fraction of the back focal plane intersecting the SP ring [see Fig. 2(a)]. The partial PSP-LDOS measurement is achieved using two motorized 50-μm multimode fibers placed in the back focal plane of the microscope [see also Ref. [32]]. We use these fibers to collect a fraction $\delta P(\omega, \mathbf{k}, \mathbf{x}_0)$ of the Fourier space in the area $\delta^2\mathbf{k}$. The radius of each fiber represents only a ratio $r = 3\%$ of the SP ring radius, meaning that only an angular ratio $r/\pi \simeq 1\%$ of the total PSP LDOS is recorded. Therefore, this method provides a way to experimentally define an angularly resolved PSP LDOS with a resolution of 1% (which could be improved by reducing the collection-fiber diameter). We define the concept of partial PSP LDOS as

$$\delta\rho_{\mathrm{PSP\ LDOS}}(\omega, \mathbf{k}, \mathbf{x}_0) \simeq \frac{3}{\pi\omega^2|\boldsymbol{\mu}|^2} I_{\mathrm{TM}}(\omega, \mathbf{k}, \mathbf{x}_0)\delta^2\mathbf{k}, \tag{3}$$

where $I_{\mathrm{TM}}(\omega, \mathbf{k}, \mathbf{x}_0)$ includes the contributions of the NSOM tip and the Bragg mirror and $\delta^2\mathbf{k} \simeq (\omega/c)^2\pi r^2$.

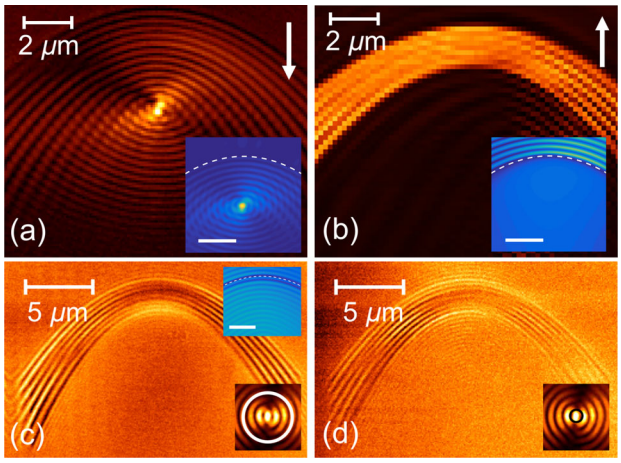

FIG. 3. (a),(b) Experimental partial PSP LDOS of the parabolic structures with an aperture NSOM tip in the classical regime for the collections in regions 1 and 2 of Fig. 2(a), respectively. The white arrow on the top-right corner indicates the collection direction. (Insets) Simulated partial PSP LDOS, scale bar 200 nm. The closest parabola to the focus point is represented by the white dashed curve. (c),(d) Experimental partial PSP LDOS obtained in the direct plane after $\mathbf{k}$ filtering with a collection fiber of 200 and 50 μm diameter, respectively. The bottom insets in (c) and (d) show a $\mathbf{k}$-filtered direct-plane image, with the corresponding collection area, taking into account the X100 magnification of the optical setup. White circle in inset (c), 2 μm diameter; black circle in inset (d), 500 nm diameter. The top inset in (c) is a simulation of the total PSP LDOS.

Partial PSP LDOS associated with two SP directions can be simultaneously recorded by means of the two collection fibers while scanning the tip over the metal film, as illustrated in Figs. 1(a) and 2(a). Figures 3(a) and 3(b) show the PSP-LDOS measurements obtained by scanning the tip over the structure focus and associated with the directions (1) and (2) depicted in Fig. 1(a), i.e., the directions where SPs are strongly reflected or weakly transmitted along the symmetry axis of the parabolas. In Fig. 3(a), a strong contrast near the focus is observed, revealing that $\delta\rho_{\mathrm{PSP\ LDOS}}(\omega, \mathbf{k}_1, \mathbf{x}_0)$ is strongly position dependent in this configuration due to the efficient SP collimation occurring with the source near the parabola focus [see Fig. 2(a)]. Conversely, $\delta\rho_{\mathrm{PSP\ LDOS}}(\omega, \mathbf{k}_2, \mathbf{x}_0)$ in Fig. 3(b) appears rather flat away from the grooves and does not depend on $\mathbf{x}_0$, in agreement with the fact that no SP collimation occurs in direction (2) [see Fig. 2(a)].

Theoretical maps of $\delta\rho_{\mathrm{SP\ LDOS}}(\omega, \mathbf{k}_1, \mathbf{x}_0)$ and $\delta\rho_{\mathrm{SP\ LDOS}}(\omega, \mathbf{k}_2, \mathbf{x}_0)$ are depicted in the insets of Figs. 3(a) and 3(b), respectively. For simplification, we modeled only one parabolic slit. The main features for each direction are very well reproduced by the simulations. $\delta\rho_{\mathrm{SP\ LDOS}}(\omega, \mathbf{k}_1, \mathbf{x}_0)$ features a maximum of intensity localized at the focus point of the parabola surrounded by fringes, while $\delta\rho_{\mathrm{SP\ LDOS}}(\omega, \mathbf{k}_2, \mathbf{x}_0)$ remains flat, in agreement with the experimental images.

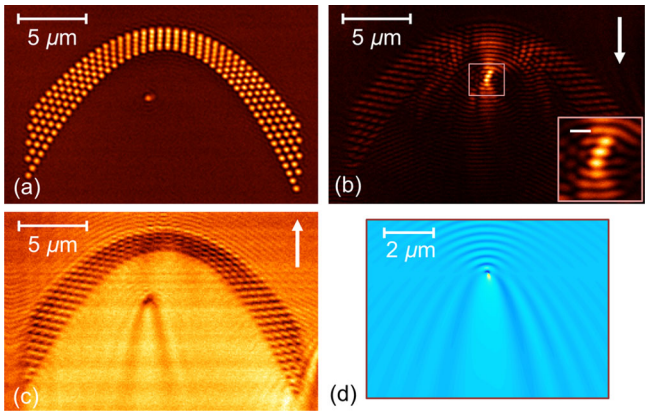

F4:1 FIG. 4. (a) Unfiltered direct plane NSOM and (b),(c) partial
F4:2 PSP-LDOS images of discretized slits forming a parabolic Bragg
F4:3 mirror that includes a nanometric defect near the focus point. The
F4:4 right arrow in the top-right corner in (b),(c) indicates the
F4:5 collection direction. [Inset in (b)] Enlargement of the focus
F4:6 point, scale bar 500 nm. (d) Simulation of PSP-LDOS images
F4:7 (c) with the nanohole only.

A similar experiment is performed with discretized parabolas made of milled nanoholes (with the diameter $d = 200$ nm). The separation between adjacent holes in a given parabola is fixed at λ_{SPP}. We show in Fig. 4(a) a transmission image when the aperture tip is located at 500 nm of the surface. We observe a defect in the metal forming a single nanohole near the focus point of the parabolas. Figures 4(b) and 4(c) present the partial PSP-LDOS measurements obtained by recording downward and upward plasmons, respectively. We see, in the first case, the same features as for the continuous parabolas of Fig. 3, i.e., a bright spot on the focus point, demonstrating that SPs are strongly reflected by the structure in the downward direction. Moreover, the effect of this collimation is so intense that the defect has no influence at all. Looking at the second partial PSP-LDOS measurement in Fig. 4(c), we see, as with the continuous parabolas, a rather flat evolution of the intensity. However, we can additionally observe an effect of the nanohole, demonstrating a kind of "hyperbolic shadowing" that results from interference between different SP contributions. The partial PSP LDOS of such a nanohole, approximated as a single dipole, has been simulated using the analytical method presented before. The resulting calculated image is shown in Fig. 4(d). The qualitative features—i.e., the hyperbolic shadowing—observed in Fig. 4(c) are again reproduced by our model.

Moreover, the above experiments can be analyzed using Lorentz's reciprocity theorem [34], which helps us to understand the images features. Indeed, this theorem has been intensively studied in the case of electromagnetic waves [34–36]. It plays a central role in nano-optics to describe and connect various NSOM and LDOS measurements [14,35,36]. In our case, the tip radially excites SPs which can be reflected by the structures. While the structure is scanned, the SPs emitted and reflected along one precise direction are collected. Applying the reciprocity theorem to this measurement amounts to exciting the structure with a (nearly perfect) plasmonic plane wave, coming from the actual collection direction. Finally, to complete the reciprocity, we have to imagine a NSOM tip in the detection mode that probes the plasmonic field above the chosen area. For parabolas, the plane wave would excite dipoles all along the slits, themselves exciting waves that would constructively interfere at the focus point. If we could scan a NSOM tip in detection mode over this area, we should obtain images very similar to what is measured in PSP LDOS (a problem which was recently analyzed using a NSOM in the detection mode [37]). For a single-hole structure, we would have a plane wave that excites a single dipole, creating a circular wave. The interference pattern obtained between a plane wave and a circular wave is typically the one obtained in Figs. 4(c) and 4(d), showing that the reciprocity theorem can be applied in this case.

It is worth emphasizing that previous LDOS measurements using NSOMs mapped the full spectrum of radiative components emitted by the tip [9,10,13,14], sometimes after filtering to keep only the "forbidden" light components [8,9,11,26,27]. Here, however, the issue is to reach enough resolution in the Fourier plane to define and map properly the partial PSP LDOS associated with specific wave vectors $\mathbf{k}$. Reaching sufficient resolution is essential for our method to be able to select a restricted part of the SP ring in order to map the PSP LDOS near the parabola focus with a very good resolution. To confirm this belief, we implement a forbidden light-LDOS measurement by mapping in the direct plane the total intensity emitted by the tip and using a $\mathbf{k}$ filter in the Fourier plane that removes components corresponding to $NA < 1$. Figures 3(c) and 3(d) show two such LDOS maps obtained with two different collection-fiber diameters. The rather flat signal confirms, in agreement with the theory [see the inset of Fig. 3(c)], that integration and averaging over the different available SP channels cancel the LDOS sensitivity to the tip position and demonstrate that the $\mathbf{k}$ resolution considered in Figs. 3(a) and 3(b) is crucial for successful PSP-LDOS mapping.

The above experiments have a simple physical interpretation, and what we show is that there is actually no backaction from the reflected plasmons on the excitation dipole, whatever its position. This absence of backaction is indeed critical for the PSP-LDOS measurement since the PSP LDOS is defined for a fixed-dipole moment. Clearly, this assumption would not be correct if the tip were near the slits. However, for points near the focus, which are relevant here, we expect that the tip is not too disturbed by the structure. Here, the SP signal reflected by the mirror and coming back on the tip could affect, in turn, the tip emission, and this situation is monitored in our experiment by detecting photons emitted near the tip

[see Figs. 3(c) and 3(d)]. The collection fiber conjugated with the sample plane discriminates against those useful photons from the background and those coming from the structure. Here, the collection fiber is represented by a circular collection area centered on the dipole. The measurement has been done with a 200-μm (50-μm) collection fiber, shown in Fig. 3(c) [Fig. 3(d)]. The inset in each figure shows the collection area, taking into account the magnification of the setup, compared to the filtered direct-plane image of the tip. In both cases, we see that the signal remains nearly constant when the tip is far away from the slit, apart from very slight modulations. Therefore, the emitting power of the tip is unchanged when we scan the structure, including in the region of interest, i.e., around the focus point.

III. APPLICATION IN THE QUANTUM REGIME

We now are in position to turn on to the quantum regime of SP excitation. We show in Fig. 5(c) the corresponding PSP-LDOS measurement with the NV-based probe excited at 532 nm, revealing the same features as in Fig. 3(b). We emphasize that the concept of PSP LDOS remains valid in the quantum regime. Indeed, above an area far from the slits, the effective dipole associated with the tip is not significantly disturbed by the SP-reflected field and therefore remains independent of its position. This result is confirmed by Fig. 3(d), which shows that the NSOM tip intensity remains constant along the plane surface, i.e., far from the slits. Moreover, for the quantum system, the NVs used as quantum emitters are in a saturation regime so that the emitted power remains constant [21].

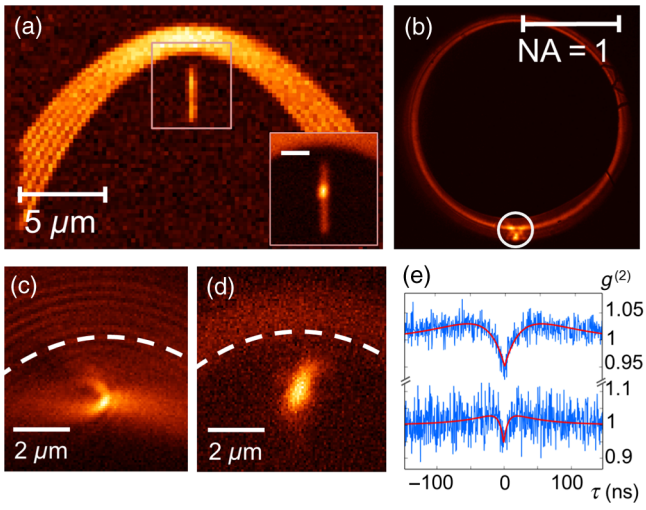

FIG. 5. Deposition of the ND at the focus point of confocal parabolas. (a) NSOM image with the tip retracted (500 nm), with a ND hosting 17 NV centers. The parabolas are the same as they were previously, but with an additional 4-μm-long slit milled through the focus point. (Inset) The ND is deposited on the slit. Scale bar, 2 μm. (b) Fourier-plane image when the deposited ND is excited. (c) Experimental quantum partial SP LDOS of the parabolas without an additional slit with the NV-based tip. (d) Scan on the structure with the deposited ND while collecting the Fourier plane in the area marked by the white circle in (b). (e) $g^{(2)}(\tau)$ functions of the ND (top chart) above glass and (bottom chart) after a dropoff in gold.

An elaborated configuration is implemented in the quantum regime to be able to measure the quantum correlation function $g^{(2)}(\tau)$ when the ND is located at the focus point above gold. The signal being very weak in the previous configuration, acquiring a $g^{(2)}(\tau)$ function by leaving the NV-based tip in a near-field height above the focus point for hours would be very challenging. Therefore, we directly deposit the ND at the focus point to excite it with the tip from the far field. The precise dropoff of the ND is assisted by a supplementary slit 4 μm long and 150 nm wide passing through the focal point and aligned with the parabola axis. Figure 5(a) presents a scan of this structure with the active tip retracted to the far field. With this tip, we catch a ND hosting 17 ± 1 NV centers [top chart of Fig. 5(e): $g^{(2)}(\tau)$ acquired above glass, showing an antibunching] and then release it at the focus point [the inset of Fig. 5(a) shows a zoom of the slit containing the ND after deposition].

In the Fourier plane image of Fig. 5(b), we still observe a strong SP collimation in the downward direction. The pattern here looks different, showing that the ND is slightly shifted away from the focus point [see the inset of Fig. 5(a)]. However, we are able to collect a large part of the collimated signal with a 200-μm-core collection fiber [the white circle in Fig. 5(b)]. The signal is strong enough to allow for a $g^{(2)}(\tau)$ measurement [the bottom chart of Fig. 5(e)]. An antibunching dip is seen, confirming that the quantum signature of the NVs has been conserved after the plasmonic propagation [22,23]. By scanning the structure in this configuration, we see in Fig. 5(d) a bright spot when the ND is excited. By fitting the $g^{(2)}(\tau)$ curves with a three-level model [38], we can extract the intrinsic photophysical parameters. The quantum efficiency Q on the glass is $Q_g = 0.40$ and increases to $Q_f = 0.63$ when the ND is located at the focus point. Therefore, the metallic structure has a strong effect on the emitter photodynamics [1,32,39].

IV. CONCLUSIONS AND PERSPECTIVES

In this article, we introduce the concept of PSP LDOS. In analogy with its previously demonstrated capability of imaging LSP LDOS in confined corrals [11], we propose an effective way to map the PSP LDOS of a parabolic Bragg collimator by means of a NSOM and a **k**-resolved LRM. Our scheme is tractable on any planar structure on a thin metal film. Using a quantum emitter and the very high contrast and resolution of our method, we are able to measure the quantum PSP LDOS and the correlation function $g^{(2)}(\tau)$, and to build a fully integrated quantum plasmonic collimator by controlling the deposition of

quantum emitters near the focus of the structure, where the PSP LDOS reaches its maximum. It is worth noting that this quantum plasmonic device is excitable in the far field using a laser source, thereby paving the way for many applications in the bottom-up development and optimization of quantum integrated devices involving SPs and quantum emitters. For instance, in addition to be well suited to probe the photodynamics of quantum emitters coupled to plasmonics systems, this method could definitely be useful in the frame of plasmon entanglement studies [40,41] and quantum nanophotonic circuitry [1,22,42].

ACKNOWLEDGMENTS

This work was supported by Agence Nationale de la Recherche (ANR), France, through SINPHONIE Grant No. ANR-12-NANO-0019 and PLACORE Grant No. ANR-13-BS10-0007. C. G. also thanks the ANR Equipex "Union" (Grant No. ANR-10-EQPX-52-01). The Ph.D. grants of A. P., by the Ministère de l'enseignement et la recherche, scientifique, and of Q. Jiang, by the Région Rhône-Alpes, are gratefully acknowledged. We thank J.-F. Motte and G. Julie, from the NANOFAB facility in Neel Institute, for sample and NSOM tip fabrication. The nanodiamond sample was provided by G. Dantelle and T. Gacoin.

[1] A. V. Akimov, A. Mukherjee, C. L. Yu, D. E. Chang, A. S. Zibrov, P. R. Hemmer, H. Park, and M. D. Lukin, Generation of single optical plasmons in metallic nanowires coupled to quantum dots, Nature (London) **450**, 402 (2007).

[2] P. Lodahl, A. F. Van Driel, I. S. Nikolaev, A. Irman, K. Obergaag, D. Vanmaekelbergh, and W. L. Vos, Controlling the dynamics of spontaneous emission from quantum dots by photonic crystals, Nature (London) **430**, 654 (2004).

[3] P. Anger, P. Bharadwaj, and L. Novotny, Enhancement and Quenching of Single-Molecule Fluorescence, Phys. Rev. Lett. **96**, 113002 (2006).

[4] S. Kühn, U. Håkanson, L. Rogobete, and V. Sandoghdar, Enhancement of Single-Molecule Fluorescence Using a Gold Nanoparticle as an Optical Nanoantenna, Phys. Rev. Lett. **97**, 017402 (2006).

[5] A. Schietinger, M. Barth, T. Aichele, and O. Benson, Plasmon-enhanced single photon emission from a nano-assembled metal-diamond hybrid structure at room temperature, Nano Lett. **9**, 1694 (2009).

[6] M. Frimmer and F. Koenderink, Spontaneous Emission Control in a Tunable Hybrid Photonic System, Phys. Rev. Lett. **110**, 217405 (2013).

[7] G. Colas des Francs, C. Girard, and A. Dereux, Theory of near-field optical imaging with a single molecule as light source, J. Chem. Phys. **117**, 4659 (2002).

[8] G. Colas des Francs, C. Girard, J. C. Weber, C. Chicane, T. David, A. Dereux, and D. Peyrade, Optical Analogy to Electronic Quantum Corrals, Phys. Rev. Lett. **86**, 4950 (2001).

[9] C. Chicanne, T. David, R. Quidant, J. C. Weber, Y. Lacroute, E. Bourillot, A. Dereux, G. Colas des Francs, and C. Girard, Imaging the Local Density of States of Optical Corrals, Phys. Rev. Lett. **88**, 097402 (2002).

[10] L. Aigouy, A. Cazé, P. Gredin, M. Mortier, and R. Carminati, Mapping and Quantifying Electric and Magnetic Dipole Luminescence at the Nanoscale, Phys. Rev. Lett. **113**, 076101 (2014).

[11] G. Colas des Francs, C. Girard, J. C. Weeber, and A. Dereux, Relationship between scanning near-field optical images and local density of photonic states, Chem. Phys. Lett. **345**, 512 (2001).

[12] R. Carminati, A. Cazé, D. Cao, F. Peragut, V. Krachmalnicoff, R. Pierrat, and Y. De Wilde, Electromagnetic density of states in complex plasmonic systems, Surf. Sci. Rep. **70**, 1 (2015).

[13] V. Krachmalnicoff, D. Cao, A. Cazé, E. Castanié, R. Pierrat, N. Bardou, S. Collin, R. Carminati, and Y. De Wilde, Towards a full characterization of a plasmonic nanostructure with a fluorescent near-field probe, Opt. Express **21**, 11536 (2013).

[14] D. Cao, A. Cazé, M. Calabrese, R. Pierrat, N. Bardou, S. Collin, R. Carminati, V. Krachmalnicoff, and Y. De Wilde, Mapping the radiative and the apparent nonradiative local density of states in the near field of a metallic nanoantenna, ACS Photonics **2**, 189 (2015).

[15] K. Imura, T. Nagahara, and H. Okamoto, Near-field two-photon-induced photoluminescence from single gold nanorods and imaging of plasmon modes, J. Phys. Chem. B **109**, 13214 (2005).

[16] F. J. Garcia de Abajo and M. Kociak, Probing the Photonic Local Density of States with Electron Energy Loss Spectroscopy, Phys. Rev. Lett. **100**, 106804 (2008).

[17] M. Kuttge, E. J. R. Vesseur, A. F. Koenderink, H. J. Lezec, H. A. Atwater, F. J. Garcia de Abajo, and A. Polman, Local density of states, spectrum, and far-field interference of surface plasmon polaritons probed by cathodoluminescence, Phys. Rev. B **79**, 113405 (2009).

[18] S. Viarbitskaya, A. Teulle, R. Marty, J. Sharma, C. Girard, A. Arbouet, and E. Dujardin, Tailoring and imaging the plasmonic local density of states in crystalline nanoprisms, Nat. Mater. **12**, 426 (2013).

[19] A. Teulle, M. Bosman, C. Girard, K. L. Gurunatha, M. Li, S. Mann, and E. Dujardin, Multimodal plasmonics in fused colloidal networks, Nat. Mater. **14**, 87 (2014).

[20] T. Coenen and A. Polman, Optical properties of single plasmonic holes probed with local electron beam excitation, ACS Nano **8**, 7350 (2014).

[21] C. Girard, O. Martin, G. Lévèque, G. Colas des Francs, and A. Dereux, Generalized bloch equations for optical interactions in confined geometries, Chem. Phys. Lett. **404**, 44 (2005).

[22] R. Kolesov, B. Grotz, G. Balasubramanian, R. J. Stöhr, A. A. L. Nicolet, P. R. Hemmer, F. Jelezko, and J. Wrachtrup, Wave-particle duality of single surface plasmon polaritons, Nat. Phys. **5**, 470 (2009).

[23] O. Mollet, S. Huant, G. Dantelle, T. Gacoin, and A. Drezet, Quantum plasmonics: Second-order coherence of surface

plasmons launched by quantum emitters into a metallic film, Phys. Rev. B **86**, 045401 (2012).

[24] M. Berthel, Q. Jiang, C. Chartrand, J. Belessa, S. Huant, C. Genet, and A. Drezet, Coherence and aberration effects in surface plasmon polariton imaging, Phys. Rev. E **92**, 033202 (2015).

[25] A. Drezet, Y. Sonnefraud, A. Cuche, O. Mollet, M. Berthel, and S. Huant, Near-field microscopy with a scanning nitrogen-vacancy color center in a diamond nanocrystal: A brief review, Micron **70**, 55 (2015).

[26] B. Hecht, H. Bielefeldt, L. Novotny, Y. Inouye, and D. W. Pohl, Local Excitation, Scattering, and Interference of Surface Plasmons, Phys. Rev. Lett. **77**, 1889 (1996).

[27] A. Bouhelier, T. Huser, H. Tamaru, H. J. Güntherodt, D. W. Pohl, F. I. Baida, and D. Van Labeke, Plasmon optics of structured silver films, Phys. Rev. B **63**, 155404 (2001).

[28] A. Drezet, D. Koller, A. Hohenau, A. Leitner, F. R. Aussenegg, and J. R. Krenn, Surface plasmon polariton microscope with parabolic reflectors, Opt. Lett. **32**, 2414 (2007).

[29] A. Drezet and C. Genet, Imaging Surface Plasmons: From Leaky Waves to Far-Field Radiation, Phys. Rev. Lett. **110**, 213901 (2013).

[30] A. Drezet, A. Hohenau, D. Koller, A. Stepanov, H. Ditlbacher, B. Steinberger, F. R. Aussenegg, A. Leitner, and J. R. Krenn, Leakage radiation microscopy of surface plasmon polaritons, Mater. Sci. Eng. B **149**, 220 (2008).

[31] P. Bharadwaj, A. Bouhelier, and L. Novotny, Electrical Excitation of Surface Plasmons, Phys. Rev. Lett. **106**, 226802 (2011).

[32] M. Berthel, S. Huant, and A. Drezet, Spatio-temporal second-order quantum correlations of surface plasmon polaritons, Opt. Lett. **41**, 37 (2016).

[33] H. Trung Dung, L. Knöll, and D.-G. Welsch, Spontaneous decay in the presence of dispersing and absorbing bodies: General theory and application to a spherical cavity, Phys. Rev. A **62**, 053804 (2000).

[34] R. Carminati, M. Nieto-Vesperinas, and J. J. Greffet, Reciprocity of evanescent electromagnetic waves, J. Opt. Soc. Am. A **15**, 706 (1998).

[35] E. R. Mendez, J.-J. Greffet, and R. Carminati, On the equivalence between the illumination and collection modes of the scanning near-field optical microscope, Opt. Commun. **142**, 7 (1997).

[36] G. Colas des Francs, C. Girard, and A. Dereux, Theory of near-field optical imaging with a single molecule as light source, J. Chem. Phys. **117**, 4659 (2002).

[37] N. Rotenberg, M. Spasenović, T. L. Krijger, B. le Feber, F. J. García de Abajo, and L. Kuipers, Plasmon Scattering from Single Subwavelength Holes, Phys. Rev. Lett. **108** 127402 (2012).

[38] M. Berthel, O. Mollet, G. Dantelle, T. Gacoin, S. Huant, and A. Drezet, Photophysics of single nitrogen-vacancy centers in diamond nanocrystals, Phys. Rev. B **91**, 035308 (2015).

[39] R. Beams, D. Smith, T. W. Johnson, S. H. Oh, L. Novotny, and A. N. Vamivakas, Nanoscale fluorescence lifetime imaging of an optical antenna with a single diamond NV center, Nano Lett. **13**, 3807 (2013).

[40] G. Di Martino, Y. Sonnefraud, M. S. Tame, S. Kéna-Cohen, F. Dieleman, Ş. K. Özdemir, M. S. Kim, and S. A. Maier, Observation of Quantum Interference in the Plasmonic Hong-Ou-Mandel Effect, Phys. Rev. Applied **1**, 034004 (2014).

[41] M.-C. Dheur, E. Devaux, T. W. Ebbesen, A. Baron, J.-C. Rodier, J.-P. Hugonin, P. Lalanne, J.-J. Greffet, G. Messin, and F. Marquier, Single-plasmon interferences, Sci. Adv. **2**, e1501574 (2016).

[42] A. G. Curto, G. Volpe, T. H. Taminiau, M. P. Kreuzer, R. Quidant, N. F. van Hulst, Unidirectional emission of a quantum dot coupled to a nanoantenna, Science **329**, 930 (2010).